Rheology of a granular gas under a plane shear

Kuniyasu Saitoh* and Hisao Hayakawa†
Department of Physics at Yoshida-South Campus, Kyoto University, Yoshida-Nihonmatsu, Sakyo, Kyoto 606-8501, Japan
(Received 24 March 2006; published 8 February 2007)

The rheology of a two-dimensional granular gas under a plane shear is investigated. From the comparison among the discrete element method, the simulation of a set of hydrodynamic equation, and the analytic solution of the steady hydrodynamic equations, it is confirmed that the fluid equations derived from the kinetic theory give us accurate results even in relatively high density cases.

DOI: 10.1103/PhysRevE.75.021302 PACS number(s): 45.70.−n, 47.57.Gc, 83.10.Pp

I. INTRODUCTION

Granular materials consist of macroscopic dissipative particles. The granular material often behaves as an unusual fluid. Although to understand the rheology of the granular fluid is practically important, our understanding on the rheology is still poor. There are several reasons to have poor understanding on the rheology of granular flows: (i) The separation of the length scale among the size of particles, the mean-free path, and the system size is not enough, (ii) there are many cases that the fluid region coexists with the solidlike region, and (iii) most of experiments are strongly affected by boundary conditions and the external field. Nevertheless, it is believed that rapid granular flows for relatively dilute granular gases can be described by a set of hydrodynamic equations derived from the kinetic theory [1].

To maintain a granular gas we need to add an external field. The simplest steady situation of the granular fluid is achieved by the balance between an external shear and inelastic collisions between particles. This system is appropriate to investigate what the constitutive equation for the granular fluid is. The kinetic theory may suggest that the relation between the stress and the strain rate at Navier-Stokes order may be sufficient to describe hydrodynamics of granular fluids [2–4].

About 50 years ago, Bagnold [5] suggested that the granular fluid is characterized by $\tau \propto \dot{\gamma}^2$ or $\eta \sim |\dot{\gamma}|$, where τ, $\dot{\gamma}$, and η are the shear stress, the shear rate (the strain rate), and the shear viscosity, respectively. This relation is known as Bagnold's scaling and is different from the conventional linear relation $\tau \propto \dot{\gamma}$. Recently, Pouliquen [6] and Silbert *et al.* [7] have reconfirmed the quantitative relevancy of Bagnold's scaling in granular flows on inclined slopes. Mitarai and Nakanishi [8] have demonstrated that a set of hydrodynamic equations at Navier-Stokes order derived from the kinetic theory can be compatible with Bagnold's scaling. Their derivation is simple. Suppose that the granular fluid can be approximated by a set of hydrodynamic equations at Navier-Stokes order. From the kinetic theory the viscosity may satisfy $\eta \propto \sqrt{T}$ with the temperature T. If there is the relation $T \propto \dot{\gamma}^2$, Bagnold's scaling $\eta \propto |\dot{\gamma}|$ is satisfied. This relation is approximately true if the heat conduction is not important in the equation of the energy continuity. Santos *et al.* [9] also indicate that Bagnold's scaling is valid for steady dilute granular gases without the influence of the gravity in the uniform shear flow (USF), though the transport coefficients such as the viscosity and the heat conductivity are different from those in homogeneous cooling state [4]. It is a key point whether the heat conduction is negligible to hold Bagnold's scaling. Therefore, it is reasonable to have Bagnold's scaling in USF because of the nonexistence of a temperature gradient. However, we still do not know whether Bagnold's scaling is relevant in other situations.

Recently, the rheology of dense granular flows under the plane shear with a constant pressure has been studied and a new scaling has been reported [10,11]. These studies are important but particles are not in a gas state, i.e., each particle is in contact with many other particles simultaneously. The analysis of such process is challenging but we do not have any good tool to analyze it at present. Here, we focus on the granular shear flows without multibody contacts in a constant volume container.

The purpose of this paper is to check the relevancy of the kinetic theory for a granular gas with moderate density under the plane shear in a constant volume container to characterize the rheology of granular fluids. For this purpose, we investigate whether (i) the kinetic theory is relevant for the granular gas and (ii) the tangential contact and the rotation of particles are irrelevant except for the boundary layers. We also discuss whether Bagnold's scaling is a universal concept for granular flows. It should be noted that Bagnold's scaling is no more relevant for flows with nonuniform shear rate in the steady granular flow without any body force. In fact, to satisfy $\tau \propto \dot{\gamma}^2$ even in an approximate sense, the shear rate $\dot{\gamma}$ should be a nearly uniform, because the shear stress and the pressure are spatially uniform in the steady state in the absence of any body force. To investigate the above problem, we use the discrete element method (DEM) for particles' simulation (Sec. II). We adopt the constitutive equations derived by Jenkins and Richman [12] for nonrotational particles in Sec. III. In Sec. IV we solve a set of hydrodynamic equations obtained from the kinetic theory numerically and compare the result with the result of DEM. We also check the renormalization theory of the restitution coefficient developed by Yoon and Jenkins [13]. In Sec. V we obtain the

*Present address: DeNA, Sasazuka, Sibuya, Tokyo, 151-0073, Japan.
†Email address: hisao@yukawa.kyoto-u.ac.jp, present address: Yukawa Institute for Theoretical Physics, Oiwake-cho, Kitashirakawa, Sakyo, Kyoto 606-8502, Japan.

analytic solution of the steady hydrodynamic equations to verify the quantitative relevancy of the constitutive equation. In Sec. VI we discuss our result and the relevancy of Bagnold's scaling. In Sec. VII, we conclude our results. In the Appendix, we briefly explain the method to determine the tangential restitution coefficient as a function of the incident angle.

II. DEM SIMULATION

A. DEM model

The discrete element method (DEM) is one of the standard methods to simulate the motion of granular particles [14]. DEM is applicable to most of situations of granular dynamics even when particles are almost motionless and in contact with many other particles simultaneously. We adopt DEM to simulate a granular fluid to check (i) the validity of kinetic theory based on the reliable model and (ii) the effects of rotation of particles for the granular fluid.

In this paper, we focus on a two-dimensional motion of granular particles under a plane shear. We adopt the linear spring model for the repulsion with the normal stiffness k_n and the tangential stiffness k_t, and the normal and the tangential viscous coefficients η_n and η_t, respectively.

Let us consider a colliding pair of two disks i and j of the diameter σ and the mass m at the position $\boldsymbol{x}_k$ with the velocity $\boldsymbol{c}_k \equiv \dot{\boldsymbol{x}}_k$ and the angular velocity $\boldsymbol{\omega}_k$ for $k=i$ or j. If the particles are in contact, the overlap distance

$$\Delta_{ij} \equiv \sigma - |\boldsymbol{x}_i - \boldsymbol{x}_j| \tag{1}$$

must be positive. The relative velocity at the contact point is given by

$$\boldsymbol{c}_{ij} = \boldsymbol{c}_i - \boldsymbol{c}_j + \frac{\sigma}{2}\boldsymbol{n}_{ij} \times (\boldsymbol{\omega}_i + \boldsymbol{\omega}_j) \tag{2}$$

with the normal unit vector $\boldsymbol{n}_{ij} \equiv (\boldsymbol{x}_i - \boldsymbol{x}_j)/|\boldsymbol{x}_i - \boldsymbol{x}_j|$. Introducing the normal velocity $c_n^{ij} = \boldsymbol{n}_{ij} \cdot \boldsymbol{c}_{ij}$, the tangential velocity $c_t^{ij} = \boldsymbol{t}_{ij} \cdot \boldsymbol{c}_{ij}$, the tangential displacement $w_t^{ij} = \int_{t_0}^{t} ds c_t^{ij}(s)$ with the tangential unit vector $\boldsymbol{t}_{ij}$ satisfying $\boldsymbol{t}_{ij} \cdot \boldsymbol{n}_{ij} = 0$, the normal and the tangential forces F_n^{ij} and F_t^{ij} are, respectively, given by

$$F_n^{ij} = mk_n\Delta_{ij} - m\eta_n v_n^{ij} \quad \text{for } \Delta_{ij} > 0, \tag{3}$$

$$F_t^{ij} = \min(h_t, \mu|F_n^{ij}|)\mathrm{sgn}(h_t^{ij}), \tag{4}$$

where $h_t^{ij} \equiv -mk_t w_t^{ij} - m\eta_t c_t^{ij}$ with Coulomb friction constant μ, $\min(a,b)$ is the function to select the smaller one between a and b, and $\mathrm{sgn}(x)=1$ for $x>0$ and $\mathrm{sgn}(x)=-1$ for $x<0$. The total repulsive force at the contact can be represented as $\boldsymbol{F}_{ij} = F_n^{ij}\boldsymbol{n}_{ij} + F_t^{ij}\boldsymbol{t}_{ij}$.

Thus, the equation of motion of particle i is described by

$$m\dot{\boldsymbol{c}}_i = \sum_{j \neq i} \boldsymbol{F}_{ij}, \tag{5}$$

$$I\dot{\boldsymbol{\omega}}_i = \frac{\sigma}{2}\sum_{j \neq i} \boldsymbol{n}_{ij} \times \boldsymbol{t}_{ij} F_t^{ij}, \tag{6}$$

where $I = m\sigma^2/8$ is the moment of inertia. We integrate Eqs. (5) and (6) in terms of the second order Adams-Bashforth with the time interval $\delta t = 4.0 \times 10^{-4}(2\sigma/U)$.

Throughout the paper we adopt the following parameters as $k_n = 3.0 \times 10^3 (U/\sigma)^2$, $k_t = k_n/4$, $\eta_n = 3.0(U/\sigma)$, $\eta_t = \eta_n/2$, and $\mu = 0.20$, where U is the relative shear speed between boundaries. These parameters lead to the normal restitution constant $\bar{e} = 0.85$ and the tangential restitution $\beta \simeq -1 + 1.12442 \cot\gamma$ for $\gamma \leq \gamma_c$ and $\beta = \beta_0 \simeq 0.769235$ for $\gamma > \gamma_c$, where γ is the incident angle of two colliding disks and the critical angle γ_c is given by $\cot\gamma_c \simeq 1.56734$ [see Eq. (A4) in the Appendix]. As shown in Appendix , the tangential restitution constant β can be approximated by [15]

$$\beta \simeq \begin{cases} -1 + \mu(1+\bar{e})\cot\gamma\left(1 + \dfrac{m\sigma^2}{4I}\right) & (\gamma \geq \gamma_c), \\ \beta_0 & (\gamma \leq \gamma_c). \end{cases} \tag{7}$$

We also note that the realistic value of Coulomb friction constant in both disks and spheres is $\mu \leq 0.2$ [16–18].

B. Setup

Simulations of granular particles under the plane shear have been performed by many researchers, but many of them [19–21] assume the Lees-Edwards boundary condition [22] which may not be adequate to consider the behavior in physical situations. On the other hand, Babic [23], Popken and Cleary [24] have simulated sheared granular flows confined in frictional flat boundaries, but their simulations are restricted to the cases for small systems and almost elastic particles. Kim [25] has indicated that the density of particles near the boundary is higher than that in the bulk region for a small system with the flat frictional boundary, while particles are accumulated in the center region for a larger system. Louge [26] has simulated a three dimensional shear flow on the flat frictional boundary to examine the boundary condition proposed by Jenkins [27], but Louge is mainly interested in the behavior of flux, the ratio of the normal stress to the shear stress as functions of volume fraction, and the restitution constant. Recent papers by Xu *et al.* for an experiment [28] and a simulation [29] examine the validity of three dimensional kinetic theory by Jenkins and Richman[30] under asymmetric shears in the presence of a streamwise body force, where they obtain reasonable agreements between the theory and the observations in both the experiment and the simulation.

To our knowledge, we do not know of any papers that discuss the validity of kinetic theory in a transient dynamics and a symmetric shear without a body force in a large enough system. Thus, we adopt the following setup of our DEM simulation shown in Fig. 1. The system is confined in a two-dimensional container. Without including the effects of the air and the gravity we add a symmetric shear with the shear speed U between two horizontal walls (Fig. 1). The fixed parameters throughout our simulation are the number

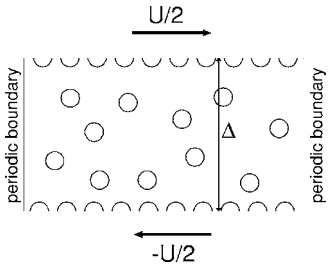

FIG. 1. The configuration of our simulation.

of particles $N=5000$, the linear dimension of the system in y direction $\Delta=180\sigma$ and the mean area fraction $\bar{\nu}=0.121$. We adopt the periodic boundary condition in the x direction which is the horizontal direction in Fig. 1.

We introduce some fixed particles on the wall to reproduce the bumpy boundary. The reason why we adopt the bumpy boundary is to avoid the large amount of slips on the wall. In our simulation we start from an initial condition without the shear. Then, the wall at $y=\Delta/2$ obeys the equation of motion in the x direction

$$M_w \frac{d\boldsymbol{c}_W}{dt} = -m\gamma_w(\boldsymbol{c}_W - U\boldsymbol{e}_x/2) + \boldsymbol{F}_{\mathrm{ex}}, \tag{8}$$

where $\boldsymbol{c}_W$ and $\boldsymbol{e}_x$ are, respectively, the actual wall velocity and the unit vector along x direction. M_w, γ_w, and $\boldsymbol{F}_{\mathrm{ex}}$ are the mass of wall $M_w=5.0\times10^6$ m, the relaxation rate $\gamma_w=10U/(2\sigma)$, and the force acting on the wall by the collision between mobile particles and the wall, respectively.

Simulation

We use the initial condition that the configuration of particles is at random and the velocity distribution function obeys Maxwellian. Figure 2 is the time evolution of particles' configuration for $\bar{\nu}=0.121$. As we can see in Fig. 2, two shallow clusters appear near the wall in an early stage, and move to the center region of the container. Then, the two clusters merge to form a big cluster. The behavior to form a big cluster can be observed in the simulation under the Lees-Edwards boundary condition [21].

The time evolution of the total kinetic energy E in a typical situation is shown in Fig. 3, where the energy is defined by

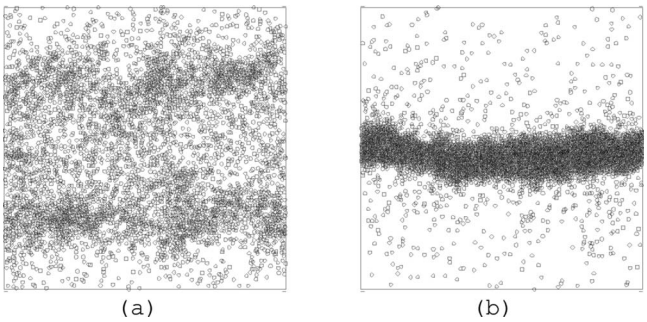

FIG. 2. The time evolution of the particles' configurations from (a) to (b) for $\bar{\nu}=0.121$.

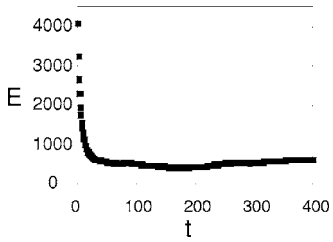

FIG. 3. The time evolution of the kinetic energy, where the units of time and the energy are $2\sigma/U$ and $mU^2/2$, respectively.

$$E(t) = \frac{1}{2}\sum_i (mc_i^2 + I\omega_i^2). \tag{9}$$

It is characteristics that the total kinetic energy is relaxed to almost a constant value quickly.

The hydrodynamic variables are the local area fraction $\nu(\boldsymbol{r},t)\equiv\pi\sigma^2 n(\boldsymbol{r},t)/4$ with the number density $n(\boldsymbol{r},t)$, the velocity field $\boldsymbol{v}(\boldsymbol{r},t)$ and the granular temperature $T(\boldsymbol{r},t)$ which is defined by

$$T(\boldsymbol{r},t) = \frac{1}{2n}\int d\boldsymbol{c}(\boldsymbol{c}-\boldsymbol{v})^2 f(\boldsymbol{r},\boldsymbol{c},t). \tag{10}$$

Unfortunately, the system size is not enough large to obtain hydrodynamic variables without neglecting x dependence. In our simulation, thus, we divide the system into rectangular cells of $\sigma\times L$ where L is the system size in x direction. Thus, the measured area fraction in our simulation is given by $\nu(y,t)\equiv\Sigma_{i\in C}\pi\sigma^2/L\sigma$ where the summation is taken over the center of particle i existing in the cell C at y. Similarly, the velocity field $\boldsymbol{v}(y,t)$ is the local average of the velocity of particles. The temperature field is also calculated by

$$T(y,t) = \frac{1}{2n}\sum_{i\in C}(\boldsymbol{c}_i - \boldsymbol{v})^2. \tag{11}$$

The time evolution of hydrodynamic variables can be summarized as follows. Corresponding to Fig. 2, the local area fraction becomes large near the boundary at the initial stage, and the shallow clusters move to the central region of the container with growing the peak density. Finally, the two dense regions merge to form a compact cluster at the center $y=0$.

The interesting behavior can be observed in the velocity field and the granular temperature. The x component of the velocity field is almost zero between two clusters during the time evolution, and such region is narrower as the distance of two clusters is closer. Even in the steady state, the velocity gradient in the central region is much smaller than that near the boundary. The y component of the dimensionless velocity field u_y is the quantity to characterize unsteady fluid motion (Fig. 4). Similarly, the temperature field in the central region is smaller than that near the boundary. However, the minimum value of temperature decreases with time and reaches almost zero in the central region in the steady stage. The results of our DEM simulation except for $u_y=2v_y/U$ will be

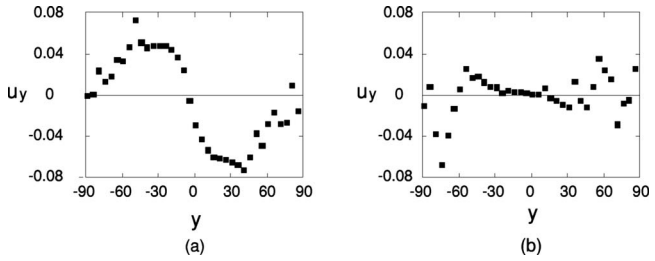

FIG. 4. The time evolution of dimensionless u_y with (a) at $t=60$ and (b) at $t=380$, where the units of the time and u_y are $(2\sigma/U)$ and $U/2$, respectively.

shown in Secs. IV and V through the comparison of DEM with hydrodynamic simulations or the theoretical results in the steady state.

The result of our simulation may give us suspicious impression of the validity of kinetic theory for this system, because (i) the density in the cluster is near the closest packing $\pi/2\sqrt{3}\simeq 0.907$ in the steady state and (ii) the particles are almost motionless in the clusters. Our result is contrast to the result by Xu *et al.* [28,29], where the flow is almost USF under the existence of a streamwise body force.

III. HYDRODYNAMIC EQUATIONS

Although there are two standard methods, Chapman-Enskog method [3,4,31] and Grad expansions [32], many of established results are limited to dilute gases to derive hydrodynamic equations from the kinetic theory. However, as shown in the previous section, we have to adopt the kinetic theory for moderate dense granular gases. Garzó and Dufty [33] and Lutsko [34] predict transport coefficients in dense granular gases based on Chapman-Enskog method. On the other hand, Jenkins and Richman derive hydrodynamic equations based on Grad expansion and give transport coefficients [12,30]. Although the treatment by Jenkins and Richman [12] does not take into account the contraction of the phase space volume in each collision, the theory is suitable for our purpose because it gives us explicit expressions of the transport coefficients in the two-dimensional dense granular gases.

Jenkins and Richman [12] and Lun [35] derive hydrodynamic equations which include the angular velocity, the spin temperature as well as the density, the translational velocity, and the granular temperature. The equations include the couple stress and the collisional loss of spin energy. These hydrodynamic equations are categorized into the micropolar fluid mechanics which was originally proposed by Cosserat and Cosserat for the description of the elastic materials [36]. Application of the concept of micropolar fluid mechanics to atomic gases are developed by Dahler and his co-workers [37]. The micropolar fluid mechanics is applied to granular flows by Kanatani [38], Lun [35], Babic [39], Hayakawa [40], and Mitarai *et al.* [41]. The importance of the excitation of the spin on the boundary is indicated by Jenkins [27], but the effects of the spin may be decoupled with the translational velocity in the bulk region. In particular, Babic [39] indicated that the coupled stress induced by the collisions between circular particles is canceled. On the other hand, some recent papers suggest that the spin effects are relevant in granular flows. For instance, Goldhirsch *et al.* [44] have indicated that the equipartition between spin energy and the translational energy is violated, and Gefen and Alam [45] discuss the linear stability of sheared micropolar fluid. Therefore, we need to judge whether the concept of micropolar fluid is necessary for the description of granular fluids.

Recently, Jenkins and Zhang [42] have suggested that the effect of the tangential contact in collisions can be absorbed in the renormalized restitution coefficient. Yoon and Jenkins [13] have extended the scheme to two-dimensional cases as

$$e \simeq \bar{e} - \mu + 2\mu^2(1+\bar{e}) \tag{12}$$

for small μ. The validity of three dimensional theory [42] has been tested by Xu *et al.* [29] and Jenkins and Zhang [42]. The latter is consistent with Lun and Bent [43] in part. However, the quantitative validity of Yoon and Jenkins [13] has not been examined yet.

In this paper, we adopt the renormalization procedure of the restitution coefficient proposed by Yoon and Jenkins [13]. Thus, the restitution constant e appears in hydrodynamic equations is different from $\bar{e}$ of DEM, where the relation between two restitution constants is given in Eq. (12). Namely, $\bar{e}=0.85$ in DEM corresponds to $e=0.798$ for $\mu=0.20$ in hydrodynamic equations.

The advantage to adopt the renormalization is that hydrodynamic equations can be simplified as

$$D_t\rho = -\rho\nabla\cdot\boldsymbol{v}, \tag{13}$$

$$\rho D_t\boldsymbol{v} = -\nabla\cdot\boldsymbol{P}, \tag{14}$$

$$\rho D_t T = -\boldsymbol{P}:(\nabla\boldsymbol{v}) - \nabla\cdot\boldsymbol{q} - \chi, \tag{15}$$

where $\rho=nm$ is the mass density and $D_t=\partial_t+\boldsymbol{v}\cdot\nabla$. Here (i,j) component P_{ij} of the pressure tensor $\boldsymbol{P}$ is expressed as the function of the bulk viscosity ξ and the shear viscosity η

$$P_{ij} = [p - \xi(\nabla\cdot\boldsymbol{v})]\delta_{ij} - \eta\hat{D}_{ij} \tag{16}$$

at the Navier-Stokes order, where $\delta_{ij}=1$ for $i=j$ and 0 for otherwise, $\hat{D}_{ij}=(\nabla_i v_j+\nabla_j v_i)/2-\delta_{ij}\nabla_k v_k/2$. Here $\boldsymbol{q}$ represents the heat flux which can be expanded as

$$\boldsymbol{q} = -\kappa\nabla T - \lambda\nabla\rho, \tag{17}$$

where κ is the heat conductivity. Note that the transport coefficient λ becomes zero at $e=1$. The collisional loss rate of the energy χ can be represented by

$$\chi = \frac{1-e^2}{4\sigma\rho_p\sqrt{\pi}}\rho^2 g(\nu)T^{1/2}[8T - 3\sqrt{\pi}\sigma T^{1/2}(\nabla\cdot\boldsymbol{v})], \tag{18}$$

where $\rho_p=4m/(\pi\sigma^2)$ is the mass density of a particle.

Let us nondimensionalize the time, position, velocity, and temperature as

TABLE I. The dimensionless transport coefficient by Jenkins and Richman.

$p(\nu)=\frac{1}{2}\nu[1+(1+e)\nu g(\nu)]$
$\xi(\nu)=\frac{1}{\sqrt{2\pi}}(1+e)\nu^2 g(\nu)$
$\eta(\nu)=\sqrt{\frac{\pi}{2}}\left[\frac{1}{7-3e}g(\nu)^{-1}+\frac{(1+e)(3e+1)}{4(7-3e)}\nu+\left(\frac{(1+e)(3e-1)}{8(7-3e)}+\frac{1}{\pi}\right)(1+e)\nu^2 g(\nu)\right]$
$\kappa(\nu)=\sqrt{2\pi}\left[\frac{1}{(1+e)(19-15e)}g(\nu)^{-1}+\frac{3(2e^2+e+1)}{8(19-15e)}\nu+\left(\frac{9(1+e)(2e-1)}{32(19-15e)}+\frac{1}{2\pi}\right)\times(1+e)\nu^2 g(\nu)\right]$
$\lambda(\nu)=-\sqrt{\frac{\pi}{2}}\frac{3e(1-e)}{16(19-15e)}[4g(\nu)^{-1}+3(1+e)\nu]\frac{1}{\nu}\frac{d(\nu^2 g(\nu))}{d\nu}$

$$t=\frac{2\sigma}{U}t^*,\quad \boldsymbol{x}=\sigma\boldsymbol{x}^*,\quad \boldsymbol{v}=\frac{U}{2}\boldsymbol{u},\quad T=\frac{U^2}{8}\theta. \tag{19}$$

Thus, the nondimensional pressure tensor, the heat flux, and the collisional loss rate of energy are, respectively, given by

$$P_{ij}=\frac{\rho_p U^2}{4}P_{ij}^*,\quad \boldsymbol{q}=\frac{\rho_p U^3}{8}\boldsymbol{q}^*,\quad \chi=\frac{\rho_p U^3}{8\sigma}\chi^*. \tag{20}$$

Here the dimensionless quantities are written as

$$P_{ij}^*=[p(\nu)\theta-\xi(\nu)\theta^{1/2}(\boldsymbol{\nabla}^*\cdot\boldsymbol{u})]\delta_{ij}-\eta(\nu)\theta^{1/2}\hat{D}_{ij}^*, \tag{21}$$

$$\boldsymbol{q}^*=-\kappa(\nu)\theta^{1/2}\boldsymbol{\nabla}^*\theta-\lambda(\nu)\theta^{3/2}\boldsymbol{\nabla}^*\nu, \tag{22}$$

$$\chi^*=\frac{1-e^2}{4\sqrt{2\pi}}\nu^2 g(\nu)\theta^{1/2}\left[4\theta-3\sqrt{\frac{\pi}{2}}\theta^{1/2}(\boldsymbol{\nabla}^*\cdot\boldsymbol{u})\right]. \tag{23}$$

The explicit expressions of $p(\nu)$, $\xi(\nu)$, $\eta(\nu)$, $\kappa(\nu)$ and $\lambda(\nu)$ obtained by Jenkins and Richman [12] are summarized in Table I with the radial distribution function [46]

$$g(\nu)=g_c(\nu)+\frac{g_f(\nu)-g_c(\nu)}{1+\exp[-(\nu-\nu_0)/m_0]}, \tag{24}$$

where $g_c(\nu)=(1-7\nu/16)/(1-\nu)^2$ and $g_f(\nu)=[(1+e)\nu(\sqrt{\nu_c/\nu}-1)]^{-1}$ with $\nu_c=0.82$, $\nu_0=0.7006$, and $m_0=0.0111$. The choice of $g(\nu)$ is not unique. For example, we expect that a similar result can be obtained by using the radial distribution function in Ref. [47]. Thus, the dimensionless hydrodynamic equations are reduced to

$$D_t\nu=-\nu\boldsymbol{\nabla}\cdot\boldsymbol{u}, \tag{25}$$

$$\nu D_t\boldsymbol{u}=-\boldsymbol{\nabla}\cdot\boldsymbol{P}, \tag{26}$$

$$\frac{1}{2}\nu D_t\theta=-P_{ij}\nabla_i u_j-\boldsymbol{\nabla}\cdot\boldsymbol{q}-\chi. \tag{27}$$

From hereon, the asterisk representing dimensionless quantities is eliminated.

IV. SIMULATION OF HYDRODYNAMIC EQUATIONS

A. The outline of our simulation

To verify the accuracy of the set of hydrodynamic equations (25)–(27) derived from the kinetic theory by Jenkins and Richman [12], we simulate hydrodynamic equations. Since the grid scale is comparable with the diameter of the disks, each grid in a two-dimensional space cannot contain enough number of particles to define hydrodynamic variables. Therefore, we average the field variables in the x direction. Thus, all quantities only depend only on y and t. However, we should note that the x component of velocity is one of the relevant hydrodynamic variables in the unsteady state. The second purpose of the simulation of hydrodynamic equations is to obtain a reduced set of equations to recover the qualitative accurate results to describe the metastable dynamics after the total energy is relaxed to a constant value.

The method of the discretization of continuous variables is based on the standard procedure. We adopt the classical Runge-Kutta scheme for the time derivative with $\delta t=0.01$ and the second order accuracy of the spatial derivative of a hydrodynamic variable Ψ as

$$\frac{\partial\Psi}{\partial y}=\frac{\Psi_{j+1}-\Psi_{j-1}}{2h},\quad \frac{\partial^2\Psi}{\partial y^2}=\frac{\Psi_{j+1}-2\Psi_j+\Psi_{j-1}}{h^2}, \tag{28}$$

where h is the grid displacement with $h/\Delta=1/180$ and $y=jh$ with $j=0,\pm1,\pm2,\ldots$. It should be noted that we do not have to solve Poisson equation for the pressure because the fluid is compressible and the pressure is completely determined by the equation of state.

B. The boundary condition

We adopt the boundary condition proposed by Johnson and Jackson [48]. We define the slip velocity on the boundary as $\boldsymbol{u}_{sl}=\boldsymbol{u}-\boldsymbol{u}_w$, where $\boldsymbol{u}_w=\pm\boldsymbol{e}_x$ at $y=\pm\Delta/(2\sigma)$. Let $\boldsymbol{t}$ and $\boldsymbol{n}$ be the tangential unit vector and the normal unit vector to the wall, respectively. Thus, the conservation of the linear momentum on the wall is given by

$$-\boldsymbol{n}\cdot\boldsymbol{P}\cdot\boldsymbol{t}=\frac{\pi}{4}\phi\Omega(\nu,\theta)|\boldsymbol{u}_{sl}|, \tag{29}$$

where $\pi/4$ is originated from $m=\pi\rho_p\sigma^2/4$. Here, ϕ is the roughness parameter and $\Omega(\nu,\theta)$ is the collisional frequency between the wall and the particles. The expression Ω is assumed to be

$$\Omega(\nu,\theta)=\nu g(\nu)\theta^{1/2}, \tag{30}$$

where the prefactor is absorbed in the roughness parameter. On the other hand, the energy balance on the wall can be expressed by

$$\boldsymbol{n}\cdot\boldsymbol{q}=-\boldsymbol{u}_{sl}\cdot\boldsymbol{P}\cdot\boldsymbol{n}-\Gamma(\nu,\theta), \tag{31}$$

where $\Gamma(\nu,\theta)$ is the energy loss rate by the inelastic collisions between particles and the wall, which may be represented as

$$\Gamma(\nu,\theta)=\frac{\Pi}{4}\Phi\Omega(\nu,\theta)\theta=\frac{\pi}{4}\Phi\nu g(\nu)\theta^{3/2}. \tag{32}$$

Here Φ is the hardness parameter of the wall. In our simulation we adopt $\phi=0.20$ and $\Phi=0.24$ as fitting parameters.

The reason why we adopt the boundary condition by Johnson and Jackson [48] is that their condition is simple.

The more precise treatment for the boundary condition can be seen in Ref. [49]. When we adopt Jenkins' boundary condition, the number of fitting parameters may be reduced.

When we represent these boundary conditions as

$$F_{b1}(\Psi, \partial_y \Psi) = 0 \tag{33}$$

and the formal solution of this discrete equation can be formally solved as

$$\Psi_N = F_{b2}(\Psi_{N-1}, \Psi_{N-2}), \tag{34}$$

where $N=\Delta/2\sigma$ is the grid number on the boundary at $y=\Delta/2\sigma$ with symbolic functions F_{b1} and F_{b2}. From the consideration of the symmetry in the y direction, we have $\nu(y)=\nu(-y)$, $\theta(y)=\theta(-y)$, and $\boldsymbol{u}(y)=-\boldsymbol{u}(-y)$. Thus, it is enough to discuss the boundary condition at $y=\Delta/2$. From Eq. (29) we may obtain the x component of the velocity field

$$u_{x;N} = \frac{u_{x;N-2} + 4\phi h \nu_{N-1} g(\nu_{N-1})/\eta(\nu_{N-1})}{1 + 4\phi h \nu_{N-1} g(\nu_{N-1}) \eta(\nu_{N-1})}, \tag{35}$$

where the area fraction ν_N on the boundary is assumed to be

$$\nu_N = 2\nu_{N-1} + \nu_{N-2} \tag{36}$$

to suppress the gradient of the density field. Similarly, Eq. (31) becomes

$$\theta_N = \frac{\theta_{N-1}\lambda(\nu_{N-1})(\nu_{N-2} - \nu_N)}{\kappa(\nu_{N-1})} + 2h\frac{[\phi(1-u_{x;N})^2 - \phi\theta_{N-1}]\nu_{N-1} g(\nu_{N-1})}{\kappa(\nu_{N-1})}. \tag{37}$$

It is obvious that y component of the velocity field satisfies

$$u_{y;N} = 0. \tag{38}$$

C. The result of numerical simulation for the complete set of hydrodynamic equations

For the initial condition to simulate hydrodynamic equations we fit the data of DEM at $t=20$ in the dimensionless unit. Each fitting curve is approximated by a polynomial of y (Fig. 5). The reason why we adopt the initial condition at $t=20$ instead of $t=0$, we are interested in the slow evolution of hydrodynamic variables after the total kinetic energy is relaxed to be a constant.

As shown in Figs. 6 and 7 the results of the simulation of hydrodynamic equations well agree with those of DEM. These agreements in the behavior between hydrodynamic equations and DEM mean that the renormalization procedure by Yoon and Jenkins [13] gives us the accurate results. Amongst hydrodynamic variables the amplitude of y component of the velocity field in the simulation of hydrodynamic equations has much larger than that of DEM though the profile itself is similar with each other. The other variables in hydrodynamic simulation are almost the same as those in DEM (Fig. 7).

It should be noted that the transient dynamics of a granular shear flow has been discussed by Babic [23] but his system is relaxed to be an USF in a small system size with small inelasticity. On the other hand, ours will not reach USF.

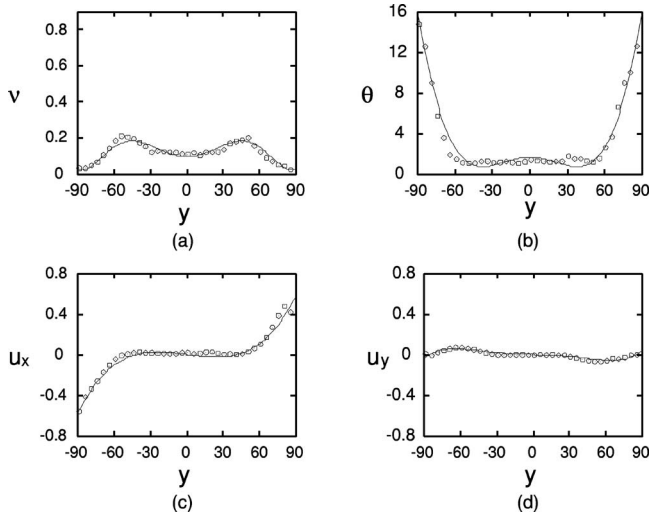

FIG. 5. The initial conditions of hydrodynamic equations (solid lines) and the corresponding data of DEM (open circles) at $t=20$, where ν, θ, u_x, u_y, and y are all dimensionless quantities (see text). The solid lines for ν and θ are the polynomials of even powers of y until y^6, while the lines for u_x and u_y are the polynomials of the odd powers of y until y^5.

D. Simulation of a simplified set of equations

To understand the qualitative behavior of phase separations, we need to reduce the degree of freedom of hydrodynamic equations. It is reasonable to deduce the terms proportional to the bulk viscosity is not important. In addition, the advection term $\boldsymbol{u}\cdot\boldsymbol{\nabla}\boldsymbol{u}$ in hydrodynamic equations may not play important roles in the plane shear problem. The coupling between the spatial gradient and the terms proportional to $1-e^2$ are also negligible, because the kinetic theory can be applied to cases for small inelasticity.

Thus, we may reduce the set of hydrodynamic equations to

$$\partial_t \nu = -\partial_y(\nu u_y), \tag{39}$$

$$\partial_t u_x = \partial_y\left[\frac{\eta(\nu)}{2}\theta^{1/2}\partial_y u_x\right], \tag{40}$$

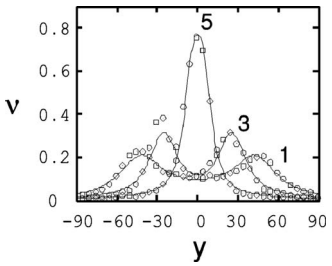

FIG. 6. The comparison of the data for the area fraction for $\bar{\nu}=0.121$ obtained by DEM (open circles) at $t=20$ (label 1), 60 (label 3), and 380 (label 5), and the result of hydrodynamic equations (25)–(27) (solid lines). Here y is the dimensionless coordinate.

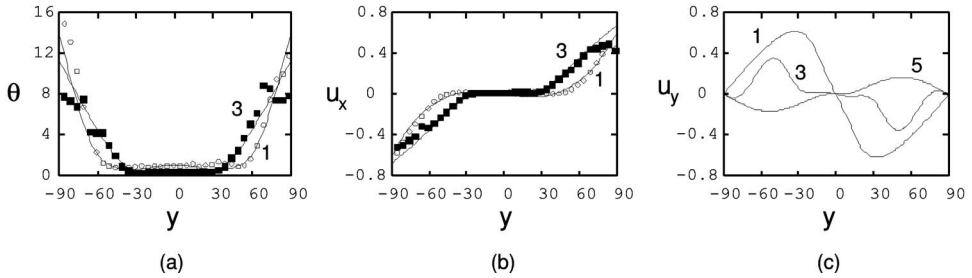

FIG. 7. The time evolution of the dimensionless temperature (a), the dimensionless velocity fields u_x (b) and u_y (c) in hydrodynamic simulations shown in solid lines, where the data in (a) and (b) are obtained by DEM. The numbers 1,3,5 in these figures correspond to results at $t=20$, 60, and 380, respectively. The DEM data with the solid squares and open circles correspond to the result at $t=20$ and 60, respectively. Note that comparison of the theory and DEM in the steady values of θ and u_x will be shown in the next section, while we do not include DEM data for u_y because of the disagreement in the scale (see Fig. 4).

$$\partial_t u_y = \partial_y[\eta(\nu)\theta^{1/2}\partial_y u_y - p(\nu)\theta], \tag{41}$$

$$\partial_t \theta = -u_y\partial_y\theta - \nu^{-1}\eta(\nu)\theta^{1/2}(\partial_y u_x)^2 + 2\nu^{-1}\eta(\nu)\theta^{1/2}(\partial_y u_y)^2 - 2\nu^{-1}\partial_y[\kappa(\nu)\theta^{1/2}\partial_y\theta] - \sqrt{2\pi}(1-e^2)\nu g(\nu)\theta^{3/2}. \tag{42}$$

For further simplification, we may assume $\partial_t\theta=0$ in Eq. (42). However, this approximation does not cause any simplification in the numerical treatment, because we still need to solve the ordinary differential equation of Eq. (42) with $\partial_t\theta=0$ in each time step. Although u_y becomes zero in the steady state, we still keep Eq. (41) in the unsteady region, because both simulations of DEM and hydrodynamics suggest that the relaxation of u_y is an important process in the slow dynamics. Thus, we believe that the set of equations (39)–(42) is the simplest set of hydrodynamic equations to describe phase separations.

Figure 8 shows the growth of hydrodynamic variables based on Eqs. (39)–(42). Although the quantitative behavior is a little deviated from the result of DEM or the full set of hydrodynamic equations (25)–(27), the qualitative behavior of this simplified model is similar to those in more accurate treatments. In the steady state both hydrodynamic models reduce to equivalent results.

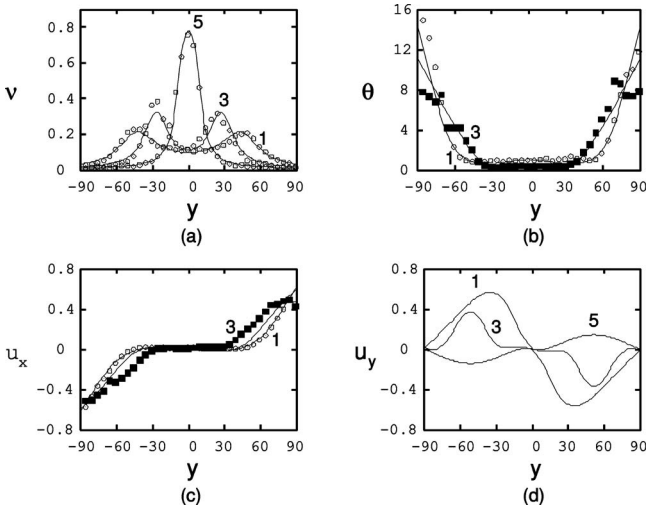

FIG. 8. The time evolution of the area fraction (a), dimensionless temperature (b), the dimensionless velocity fields u_x (c) and u_y (d) in the simulation of a simplified model (42) of hydrodynamic equations. The numbers 1,3,5 in these figures correspond to the data at $t=20$, 60, and 380, respectively.

V. THEORETICAL DESCRIPTION OF THE STEADY STATE

In the steady state, the hydrodynamic variables depend only on y. Thus, the variables are

$$\nu = \nu(y),\ u_x = u_x(y),\ u_y = 0,\ \theta = \theta(y). \tag{43}$$

It is obvious that any hydrodynamic variable Ψ satisfies $D_t\Psi = \partial_t\Psi = 0$. Thus, the equation of mass conservation is automatically satisfied. The relevant equations of motion become

$$0 = \frac{d}{dy}P_{xy}, \tag{44}$$

$$0 = \frac{d}{dy}P_{yy}, \tag{45}$$

$$0 = P_{yx}\frac{d}{dy}u_x + \frac{d}{dy}q_y + \chi. \tag{46}$$

Thus, the normal stress and the shear stress are uniform

$$p \equiv P_{yy} = \text{const}, \quad \tau \equiv P_{yx} = \text{const}. \tag{47}$$

From the definition of the pressure tensor we obtain

$$\tau = -\frac{\eta(\nu)}{2}\theta^{1/2}\frac{du_x}{dy}, \tag{48}$$

$$p = \frac{1}{2}\nu[1 + (1+e)\nu g(\nu)]\theta. \tag{49}$$

Thus, we obtain the expressions for θ and du_x/dy as functions of p, τ and ν. Substituting them into the last equation of (46) we obtain

$$\frac{d}{dy}\left[F(\nu)\frac{d\nu}{dy}\right] = G(\nu), \tag{50}$$

where

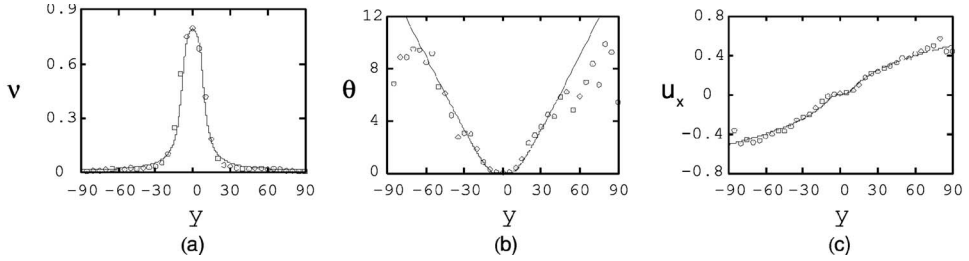

FIG. 9. The comparison between theory (solid lines) and DEM simulation without the tangential interaction (open circles) for area fraction (a), dimensionless temperature (b), and u_x (c). The mean area fraction is $\bar{\nu}=0.121$.

$$F(\nu)=\frac{1}{\alpha(\nu)^{3/2}}\left[\left(\frac{1}{2}+r\frac{d}{d\nu}(\nu^2 g)\right)\frac{\kappa(\nu)}{\alpha(\nu)}-\lambda(\nu)\right], \quad (51)$$

$$G(\nu)=\epsilon\frac{2\alpha(\nu)^{1/2}}{\eta(\nu)}-(1-e)\frac{\xi(\nu)}{\alpha(\nu)^{3/2}} \quad (52)$$

with $\epsilon=(\tau/p)^2$ and $\alpha(\nu)=2/\{\nu[1+(1+e)\nu g(\nu)]\}$.

It is well established how to solve a second order ordinary differential equation such as Eq. (50). Introducing $H(\nu)$ as $dH(\nu)/d\nu=F(\nu)$ and the multiplying dH/dy in both sides of Eq. (50), and thus integrate the equation from $y=0$ to y we obtain

$$\frac{1}{2}\left(\frac{dH}{dy}\right)^2=\int_{\nu(0)}^{\nu(y)}d\nu F(\nu)G(\nu), \quad (53)$$

where we use the symmetric condition $d\nu/dy=dH/dy=0$ at $y=0$.

$$\pm\int_{\nu(0)}^{\nu(y)}\frac{F(\nu)}{\sqrt{2\int_{\nu(0)}^{\nu}F(\nu')G(\nu')d\nu'}}d\nu=y. \quad (54)$$

Thus, we obtain the equation of y as the function of ν.

To draw the actual profile of ν, we start from a trial $\nu_1(0)$ to integrate Eq. (54) and calculate $I_1=\int_{-\Delta/2}^{\Delta/2}\nu_1(y)dy$, where the suffix 1 represents the first trial function. Then we replace $\nu_1(0)$ by $\nu_2(0)$ to reduce the deviation between I_1 and $\bar{\nu}$. We repeat this relaxation procedure to obtain the converged result $I_M\to\bar{\nu}$ until Mth trial. Once we obtain ν, we can determine θ and du_x/dy by Eq. (48).

To compare ν and du_x/dy with the result of DEM we use a fitting parameter $\epsilon=(\tau/p)^2$, while we need two fitting parameters ($\tau=-0.0017$ and $p=0.1$ for nonrotational cases and $\tau=-0.0017$ and $p=0.06$ for rotational cases) to determine u_x and θ. It should be noted that p and τ are determined by the boundary condition, but the boundary condition in Eqs. (29) and (31) with Eq. (32) contains two undetermined parameters. Thus, p and τ cannot be determined within our theory.

Figure 9 is the comparison of our theoretical result with the result of DEM without the tangential contact force in the interaction between particles for $\bar{\nu}=0.121$. The agreement between the theory and DEM is good. Figure 10 is the comparison of our theoretical result with the result of DEM with the tangential interaction for $\bar{\nu}=0.121$. We again obtain a fairly good agreement between the theory and the simulation.

The reason why we can use the kinetic theory is that collisions between particles are almost binary even in the dense cluster. Actually, we find that contacted particles are about 1.014% of all particles at an instance, and only 2.4% of contacts are multibody contacts among all contacts for $\bar{\nu}=0.121$. Therefore, the kinetic theory can be used even in the dense cluster in which particles are almost motionless.

In principle, we can measure both the normal stress and the shear stress from the data of DEM. However, we only obtain the results with large errors. It seems that there is a tendency to have too small p in the direct measurement, though observed τ is similar to the fitting value.

Thus, we confirm that (i) the kinetic theory by Jenkins and Richman [12] can reproduce the profiles of hydrodynamic variables to describe the steady state of the granular fluid though the fitting values of the stresses are included and (ii) the renormalization scheme proposed by Yoon and Jenkins [13] is accurate. Although the setup of our simulation seem to be similar to that by Xu *et al.* [29], our result for hydrodynamic variables is much heterogeneous than that by Xu *et al.* in the presence of a streamwise flow. In fact, our system is separated into two regions which are a compact cluster and the very dilute region. The particles within the cluster is almost motionless, but the particles in the dilute region have large kinetic energy. On the other hand, the steady state obtained by Xu *et al.* [29]. is similar to USF. Thus, the result strongly depends on whether there is a stream flow.

VI. DISCUSSION

Let us discuss our results. One of the main purposes of this paper is to clarify whether Bagnold's scaling is universal

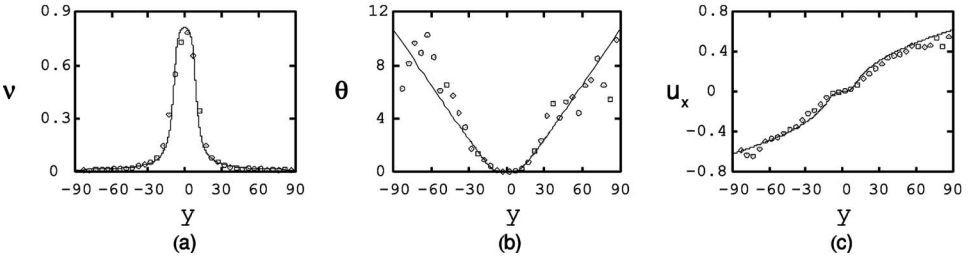

FIG. 10. The comparison between theory (solid lines) and DEM simulation with the tangential interaction (open circles) for area fraction (a), dimensionless temperature (b), and u_x (c). Here we use $e=0.798$ and the mean area fraction $\bar{\nu}=0.121$.

in granular flows. Our result is one of counter examples of Bagnold's scaling in sheared granular fluids because the shear rate strongly depends on the position but the shear stress is uniform.

One of most important points is that our system does not contain any external body force. In physical situations, to remove the effect of gravity is difficult. In the presence of an external field, the energy is directly supplied to particles where the heat conduction does not play any role, while the energy is transferred from the boundary in terms of the heat conduction in our system. As a result, Bagnold's scaling for systems in the presence of an external body force seems to be valid [6,8,64]. On the other hand, the heat conduction is important for our system in which Bagnold's scaling is not satisfied. We can stress that particles are almost motionless in the bulk region where the influence of the heat conduction is small.

Even when the system is compressed by the external pressure, the main fraction of the energy is transferred not by the heat conduction but by the elastic wave. Therefore, Bagnold's scaling may be observed in some parameter regions even in such systems. As indicated in Introduction, however, recent papers and references cited therein [10,11] of sheared granular materials under a constant pressure produce a state of "granular liquid" has a new scaling region. This is because the pressure and the stiffness of grains which becomes important because of multiple contacts of particles produce another time scale. Thus, the behavior can depend on the shear rate.

On the other hand, the situation of granular shear flows confined in a periodic boundary condition which satisfies Lees-Edwards boundary condition is more controversial. Since a nonuniform shear flow produces a heat conduction, Bagnold's scaling may not be satisfied if the USF is unstable. The stability of the USF under the Lees-Edwards boundary condition has been studied by many authors [50–60]. These results suggest that USF is almost always unstable but (a) if the system is confined in a small system near $e \to 1$ and (b) if the gas system is in the dilute limit or in the almost dense limit, stable USF can be observed. These results may suggest that Bagnold's scaling is only applicable in the limited cases for plane shears.

In this paper, we used the set of hydrodynamic equations at Navier-Stokes order which does not have any normal-stress differences. Although such differences may be related to the existence of Burnett or super-Burnett order terms [58,61,62], we cannot evaluate how large higher order terms are because of large errors in the direct measurement of stresses in our simulation. However, such higher order terms should not be important in our system, because our analysis without including higher order terms recovers the profile of hydrodynamic variables.

From our analysis, we confirm that the effects from the contraction of phase volume in collisions in the inelastic Boltzmann-Enskog equation are also small. The effects of tangential contact force and the rotation of particles are also not important in the bulk behavior of hydrodynamics. Therefore, the kinetic theory by Jenkins and Richman [12] gives us sufficiently accurate results to describe the hydrodynamics.

Santos *et al.* [9] and Tij *et al.* [63] indicate that the transport coefficients in Couette flow depend on the dimensionless shear rate. However, in our system the shear rate only determines the time scale and thus the qualitative behavior should not depend on the shear rate. There is room for discussion on the role of the shear rate in granular gases as an open problem.

VII. CONCLUSION

In this paper, we have confirmed the validity of hydrodynamic equations derived from the kinetic theory by Jenkins and Richman [12]. We also confirmed the relevancy of the renormalization method of the restitution constant by Yoon and Jenkins [13]. This result may be surprising because the system includes a dense cluster whose packing fraction is close to the maximum value, and the particles in the cluster are almost motionless. Since USF is unstable under a plane shear with the physical boundary, we cannot use Bagnold's scaling to characterize the granular fluid in this case.

ACKNOWLEDGMENTS

We thank N. Mitarai and T. Hatano for fruitful discussion and their variable comments. H.H. also thanks J. T. Jenkins for his useful comments. This study was partially supported by the Grants-in-Aid of Japan Space Forum, and Ministry of Education, Culture, Sports, Science and Technology (MEXT), Japan (Grant Nos. 15540393 and 18540371) and the Grant-in-Aid for the 21st century COE "Center for Diversity and Universality in Physics" from MEXT, Japan.

APPENDIX: THE DERIVATION OF WALTON'S β_0

In this appendix, we demonstrate how to derive β_0 in Walton's expression in Eq. (7) [15] for the tangential restitution coefficient. Although the theory by Maw *et al.* [16,18,65,66] has been used to evaluate β, their expression is complicated and has an implicit form. Therefore, an explicit expression for Walton's β_0 and the critical angle γ_c is useful.

Let us consider a collision between identical disks. Following the notation in Sec. II (without suffices i and j for colliding particles), the equation of motion for the tangential direction is described by

$$\ddot{w}_t + 2(\eta_t \dot{w}_t + k_t w_t) = 0, \tag{A1}$$

when there is no slip during the collision. The factor 2 appears because the reduced mass is the half of mass of each particle. The solution of Eq. (A1) is easily obtained as

$$w_t = \frac{w_t(0)}{b} e^{-\eta_t t} \sin(bt),$$

$$\dot{w}_t(t) = w_t(0) e^{-\eta_t t} \left(\cos(bt) - \frac{\eta_t}{b} \sin(bt) \right) \tag{A2}$$

for $\eta_t^2 < 2k_t$, where $b = \sqrt{2k_t - \eta_t^2}$.

Since we choose large k_t and small η_t, the relation $\eta_t^2 < 2k_t$ should be satisfied. Similarly, the equation of motion in the normal direction is also described by an equation for a dumped oscillation. Thus, the duration time t_d at which w_n

=0 is satisfied and the normal restitution constant are, respectively, given by

$$t_d = \frac{2\pi}{\sqrt{2k_n - \eta_n^2}}, \quad \bar{e} = \exp\left[-\frac{\pi\eta_n}{\sqrt{2k_n^2 - \eta_n^2}}\right]. \tag{A3}$$

On the other hand, the restitution constant β_0 for the tangential contact is thus given by

$$\beta_0 = -\frac{\dot{w}_t(t_d)}{\dot{w}_t(0)} = \exp\left(-\frac{\pi A\,\eta_t}{\eta_n\sqrt{2R-1}}\right) \times\left[\frac{1}{\sqrt{2Q/A-1}}\sin\left(\frac{\pi A\,\eta_t\sqrt{2Q/A-1}}{\eta_n\sqrt{2R-1}}\right) - \cos\left(\frac{\pi A\,\eta_t\sqrt{2Q/A-1}}{\eta_n\sqrt{2R-1}}\right)\right], \tag{A4}$$

where

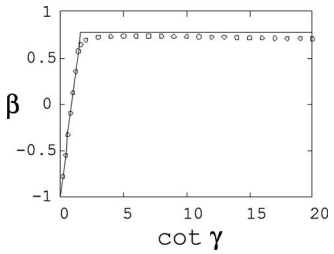

FIG. 11. The comparison of Eq. (7) with (A4) (solid line) and the data obtained from DEM with $\mu=0.2$ (open circles). Here β and γ are respectively the tangential restitution coefficient and the collision angle.

$$A = 1 + \frac{m\sigma^2}{4I},\ R = \frac{\pi k_n}{4\eta_n^2},\ Q = \frac{\pi k_t}{4\eta_t^2}. \tag{A5}$$

If we substitute the values $k_n=3.0\times10^3$, $k_t=k_n/4$, $\eta_n=3.0$ and $\eta_t=\eta_n/2$ used in the DEM simulation, we obtain $\beta_0 \simeq 0.769235$. The comparison between the theory (7) with (A4) and DEM is shown in Fig. 11. Without the introduction of any fitting parameters, agreement between the theory and DEM is fairly good. Here the critical angle $\cot\gamma_c=(1+\beta_0)\mu(1+\bar{e})\simeq 1.56734$.

[1] I. Goldhirsch, Annu. Rev. Fluid Mech. **35**, 267 (2003).
[2] *Granular Gases*, edited by T. Pöschel and S. Luding (Springer-Verlag, Berlin, 2001).
[3] N. V. Brilliantov and T. Pöschel, *Kinetic Theory of Granular Gases* (Oxford University Press, Oxford, 2004).
[4] J. J. Brey, J. W. Dufty, C. S. Kim, and A. Santos, Phys. Rev. E **58**, 4638 (1998).
[5] R. A. Bagnold, Proc. R. Soc. London, Ser. A **225**, 49 (1954).
[6] O. Pouliquen, Phys. Fluids **11**, 542 (1999).
[7] L. E. Silbert, D. Ertas, G. S. Grest, T. C. Halsey, D. Levine, and S. J. Plimton, Phys. Rev. E **64**, 051302 (2001).
[8] N. Mitarai and H. Nakanishi, Phys. Rev. Lett. **94**, 128001 (2005).
[9] A. Santos, V. Garzó, and J. Dufty, Phys. Rev. E **69**, 061303 (2004).
[10] G. D. R. Midi, Eur. Phys. J. E **14**, 341 (2004).
[11] F. da Cruz, S. Eman, M. Prochnow, J.-N. Roux, and F. Chevoir, Phys. Rev. E **72**, 021309 (2005).
[12] J. T. Jenkins and M. W. Richman, Phys. Fluids **28**, 3485 (1985).
[13] D. K. Yoon and J. T. Jenkins, Phys. Fluids **17**, 083301 (2005).
[14] P. A. Cundall and O. D. L. Strack, Geotechnique **29**, 47 (1979).
[15] O. R. Walton and R. L. Braun, J. Rheol. **30**, 949 (1986).
[16] W. J. Stronge, *Impact Mechanics* (Cambridge University Press, London, 2000).
[17] L. Labous, A. D. Rosato, and R. N. Dave, Phys. Rev. E **56**, 5717 (1997).
[18] H. Kuninaka and H. Hayakawa, J. Phys. Soc. Jpn. **72**, 1655 (2003).
[19] C. S. Campbell, J. Fluid Mech. **348**, 85 (1997).
[20] R. N. Dave, A. D. Rosato, and K. Bhaswan, Mech. Res. Commun. **22**, 335 (1995).
[21] M.-L. Tan and I. Goldhirsch, Phys. Fluids **9**, 856 (1997).
[22] A. W. Lees and S. F. Edwards, J. Phys. C **5**, 1921 (1972).
[23] M. Babic, Phys. Fluids **9**, 2486 (1997).
[24] L. Popken and P. W. Cleary, J. Comput. Phys. **155**, 1 (1999).
[25] S. R. Kim, Comput. Mater. Sci. **4**, 125 (1995).
[26] M. Y. Louge, Phys. Fluids **6**, 2253 (1994).
[27] J. T. Jenkins, J. Appl. Mech. **59**, 120 (1992).
[28] H. Xu, A. P. Reeves, and M. Y. Louge, Rev. Sci. Instrum. **75**, 811 (2004).
[29] H. Xu, M. Y. Louge, and A. P. Reeves, Continuum Mech. Thermodyn. **15**, 321 (2003).
[30] J. T. Jenkins and M. W. Richman, Arch. Ration. Mech. Anal. **87**, 355 (1985).
[31] S. Chapman and Cowling, *The Mathematical Theory of Non-uniform Gases*, 3rd ed. (Cambridge University Press, Cambridge 1970).
[32] H. Grad, Commun. Pure Appl. Math. **2**, 331 (1949).
[33] V. Garzó and J. W. Dufty, Phys. Rev. E **59**, 5895 (1998).
[34] J. F. Lutsko, Phys. Rev. E **72**, 021306 (2005).
[35] C. K. K. Lun, J. Fluid Mech. **233**, 539 (1991).
[36] E. Cosserat and F. Cosserat, *Theorie des Crops Deformables* (Herrmann, Paris 1960).
[37] J. S. Dahler and M. Theodosopulu, Adv. Chem. Phys. **31**, 155 (1975).
[38] K. Kanatani, Trans. Jpn. Soc. Mech. Eng., Ser. B **45**, 507 (1979).
[39] M. Babic, Int. J. Eng. Sci. **35**, 523 (1997).
[40] H. Hayakawa, Phys. Rev. E **61**, 5477 (2000).
[41] N. Mitarai, H. Hayakawa, and H. Nakanishi, Phys. Rev. Lett. **88**, 174301 (2002).
[42] J. T. Jenkins and C. Zhang, Phys. Fluids **14**, 1228 (2002).

[43] C. K. K. Lun and A. A. Bent, J. Fluid Mech. **258**, 335 (1994).
[44] I. Goldhirsch, S. H. Noskowicz, and O. Bar-Lev, Phys. Rev. Lett. **95**, 068002 (2005).
[45] B. Gefen and M. Alam, J. Fluid Mech. **567**, 195 (2006).
[46] D. Volfson, L. S. Tsimring, and I. S. Aranson, Phys. Rev. E **68**, 021301 (2003).
[47] S. Torquato, Phys. Rev. E **51**, 3170 (1995).
[48] P. C. Johnson and R. Jackson, J. Fluid Mech. **176**, 67 (1987).
[49] J. T. Jenkins, in Ref. [2], pp. 125–139. See also J. T. Jenkins and M. W. Richman, J. Fluid Mech. **171**, 53 (1986).
[50] M. Latzel, S. Luding, and H. J. Herrmann, Granular Matter **2**, 123 (2000).
[51] P. R. Nott, M. Alam, K. Agrawal, R. Jackson, and S. Sundaresan, J. Fluid Mech. **397**, 203 (1999).
[52] M. Alam and P. R. Nott, J. Fluid Mech. **377**, 99 (1998).
[53] M. Alam and P. R. Nott, J. Fluid Mech. **343**, 267 (1997).
[54] M. Babic, J. Fluid Mech. **254**, 127 (1993).
[55] S. A. Kinnas and N. E. Fine, J. Fluid Mech. **254**, 151 (1993).
[56] C. Wang, R. Jackson, and S. Sundaresan, J. Fluid Mech. **308**, 31 (1996).
[57] S. B. Savage, J. Fluid Mech. **241**, 109 (1992).
[58] V. Kumaran, J. Fluid Mech. **506**, 1 (2004).
[59] V. Garzó, Phys. Rev. E **73**, 021304 (2006).
[60] K. Saito and H. Hayakawa (unpublished).
[61] N. Sela, I. Goldhirsch, and S. H. Noskowicz, Phys. Fluids **8**, 2337 (1996).
[62] N. Sela and I. Goldhirsch, J. Fluid Mech. **361**, 41 (1998).
[63] M. Tij, E. E. Tahiri, J. M. Montanero, V. Garó, A. Santos, and J. W. Dufty, J. Stat. Phys. **103**, 1035 (2001).
[64] C. Josserand, P.-Y. Lagrée, and D. Lhuillier, Eur. Phys. J. E **14**, 127 (2004).
[65] N. Maw, R. Barber, and J. N. Fawcett, Wear **38**, 101 (1976).
[66] N. Maw, R. Barber, and J. N. Fawcett, ASME J. Lubr. Technol. **103**, 74 (1981).